International Journal of Nanomedicine

Dovepress

open access to scientific and medical research

Open Access Full Text Article

ORIGINAL RESEARCH

TiO_2-Ti_3C_2 Nanocomposites Utilize Their Photothermal Activity for Targeted Treatment of Colorectal Cancer

Zhenlei Wang[1], Zengci Run[1], Huamin Wang[2], Xiaojun He[3], Jian Li[1]

[1]Department of General Surgery, The Affiliated Cancer Hospital of Zhengzhou University & Henan Cancer Hospital, Zhengzhou, Henan, 450008, People's Republic of China; [2]Department of Pediatrics, Second Affiliated Hospital & Yuying Children's Hospital of Wenzhou Medical University, Wenzhou, Zhejiang, 325027, People's Republic of China; [3]School of Ophthalmology & Optometry School of Biomedical Engineering Wenzhou Medical University, Wenzhou, Zhejiang, 325035, People's Republic of China

Correspondence: Jian Li, Department of General Surgery, The Affiliated Cancer Hospital of Zhengzhou University & Henan Cancer Hospital, No. 127 Dongming Road, Jinshui District, Zhengzhou, Henan, 450008, People's Republic of China, Tel +86 18638927768, Email garfycat@126.com; Xiaojun He, School of Ophthalmology & Optometry School of Biomedical Engineering Wenzhou Medical University, Wenzhou, Zhejiang, 325035, People's Republic of China, Tel +86 15626166187, Email 513080867@qq.com

Purpose: The search for effective and low-risk treatment methods for colorectal cancer (CRC) is a pressing concern, given the inherent risks and adverse reactions associated with traditional therapies. Photothermal therapy (PTT) has emerged as a promising approach for cancer treatment, offering advantages such as non-radiation, non-invasiveness, and targeted treatment. Consequently, the development of nanoparticles with high stability, biocompatibility, and photothermal effects has become a significant research focus within the field of PTT.

Methods: In this study, TiO_2-Ti_3C_2 nanocomposites were synthesized and characterized, and their photothermal conversion efficiency in the near-infrared region II (NIR-II) was determined. Then studied the in vivo and in vitro photothermal activity and anti-tumor effect of TiO_2-Ti_3C_2 in human colorectal cancer cell lines and nude mice subcutaneous tumor model.

Results: The results showed that TiO_2-Ti_3C_2 nanocomposites have strong absorption ability in the NIR-II, and have high photothermal conversion efficiency under 1064 nm (0.5 W/cm^2, 6 min) laser stimulation. In addition, in vitro experiments showed that TiO_2-Ti_3C_2 nanocomposites significantly inhibited the invasion, migration, and proliferation of colorectal cancer cells, and induced cell apoptosis; in vivo, experiments showed that TiO_2-Ti_3C_2 nanocomposites-mediated PTT had good biocompatibility and efficient targeted inhibition of tumor growth.

Conclusion: In conclusion, TiO_2-Ti_3C_2 nanocomposites can be used as NIR-II absorption materials in PTT to suppress the invasion, migration, and proliferation of colorectal cancer cells, induce colorectal cancer cell apoptosis, and thus inhibit the development of CRC. Therefore, TiO_2-Ti_3C_2 nanocomposites can be used as potential anti-tumor drugs for photothermal ablation of colorectal cancer cells.

Keywords: TiO_2-Ti_3C_2, photothermal activity, colorectal cancer, photothermal therapy

Introduction

Colorectal cancer (CRC) remains a significant contributor to mortality from malignant diseases in humans.[1] According to the 2020 GLOBOCAN statistics, there were approximately 19.3 million new cancer cases globally, with a CRC incidence rate of 10.0%, ranking third among all cancer incidence rates, following breast cancer (11.7%) and lung cancer (11.4%). In terms of mortality rates, over 10 million cancer-related deaths were reported, with CRC accounting for 9.4% of all cancer deaths, second only to lung cancer.[2] The survival rate of CRC patients is notably low, with stage IV cases having a survival rate of less than 20%.[1,3] Traditional treatments for CRC include surgery, radiotherapy, and chemotherapy, but often come with side effects such as intestinal dysfunction, bladder dysfunction, and sexual dysfunction.[1,4–6] Studies have shown that CRC survivors have a higher incidence of sexual dysfunction compared to survivors of other cancers.[7]

Received: 25 October 2023
Accepted: 11 January 2024
Published: 1 February 2024

Graphical Abstract

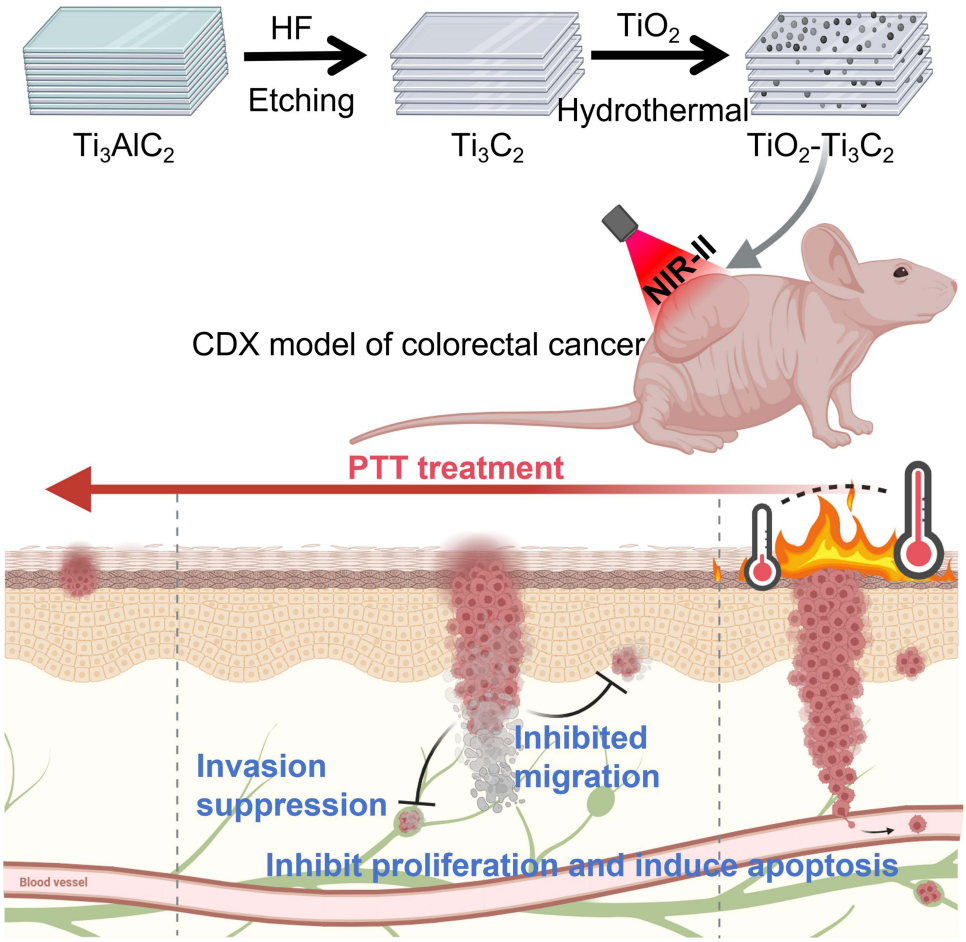

The high incidence, low survival rate, and associated adverse reactions of traditional treatment methods continue to present significant challenges in the clinical management of CRC. Therefore, the development of an efficient low-side-effect treatment method is urgently needed.

In recent years, nanoparticle-based photothermal therapy (PTT) has emerged as a promising approach in the treatment of CRC. Nanomaterials such as poly[2-(N,N-dimethylamino) ethyl methacrylate]-poly(ε-caprolactone), Au-Ag, and GNC-Gal@CMaP exhibit excellent photothermal conversion efficiency when irradiated with 808 nm laser and play a role in the treatment of CRC through synergistic effects with other molecules or drugs.[8–10] PTT represents an ideal non-invasive treatment modality, leveraging an external light source to activate photothermal agents and induce localized thermal therapy that irreversibly damages tumor cells.[11] Near-infrared (NIR) light has demonstrated excellent tissue penetration capabilities, making it highly promising for clinical diagnosis and disease treatment in PTT.[12–14] NIR light is classified into two regions: NIR-I (750–1000 nm) and NIR-II (1000–1350 nm), collectively forming the biological window due to their ability to penetrate biological tissue.[12] The NIR-II biological window, in particular, offers deeper tissue penetration, higher radiation limits, and better tissue tolerance, making it highly valuable for photothermal conversion applications.[12,13] The key to the application of NIR-II absorption materials in PTT is that the material should have excellent photothermal conversion efficiency, low toxicity, and good biocompatibility.[12,15] However, current research predominantly utilizes NIR-I absorption materials in PTT for CRC, while investigations on NIR-II absorption

materials remain relatively limited.[8–10] Therefore, the development of nanomaterials with strong absorption within the NIR-II biological window and high photothermal conversion efficiency holds significant importance for CRC treatment.

Two-dimensional MXene nanomaterials, such as titanium carbide (Ti_3C_2), have been widely used in biomedical applications due to their excellent NIR absorption, photothermal performance, and low toxicity, making Ti_3C_2 a potential photothermal agent.[16] TiO_2 is a highly efficient, stable, and environmentally-friendly photocatalytic material.[17] It possesses remarkable photosensitivity, favorable thermal stability, and biocompatibility.[17–20] Research has indicated that the application of TiO_2 modification can lead to enhanced biocompatibility and stability of TiC_3.[17–20] Furthermore, reports suggest that the photothermal performance of other nanomaterials (such as porous silicon) can be improved by encapsulating them with TiO_2, but there is no relevant report on whether TiO_2 can improve the photothermal performance of Ti_3C_2.[21] It is worth mentioning that Ti_3C_2 exhibits significant NIR-I (808 nm) absorption capabilities,[22,23] while the Ti_3C_2@TiO_2-x-PEG composite material demonstrates high photothermal conversion efficiency when irradiated with NIR-II (1064 nm) laser.[16] Therefore, TiO_2-Ti_3C_2 composites hold potential as NIR-II absorption materials and could be employed in PTT for CRC. However, existing research predominantly focuses on the photocatalytic properties of TiO_2-Ti_3C_2 composites, with limited investigations on their photothermal properties. Moreover, the in vivo and in vitro photothermal activity of TiO2-Ti3C2 composites remains unexplored. Conducting corresponding in vivo and in vitro studies to explore the application value of TiO_2-Ti_3C_2 composites in targeted PTT for colorectal cancer is of great significance for promoting research in this field.

Based on this, we first synthesized Ti_3C_2 MXenes and TiO_2-Ti_3C_2 nanocomposites and comprehensively analyzed their characterization and photothermal conversion efficiency. Subsequently, we conducted studies at the cellular and animal levels to reveal the role of nanocomposites in targeted PTT for CRC. Human colorectal cancer cell lines and nude mouse subcutaneous tumor models were used to investigate the anti-tumor effects of TiO_2-Ti_3C_2.

Materials and Methods

Synthesis and Characterization of Ti_3C_2 and TiO_2-Ti_3C_2

Synthesis of Ti_3C_2 MXene. Firstly, 5.0 g of Ti_3AlC_2 (Aladdin, China) powder was added to 80 mL of 40% HF (Aladdin, China) solution and stirred at room temperature for 48 hours to obtain the MXene suspension. The resulting suspension was washed 6 times with deionized water and centrifuged at 4000 rpm to separate the powder until the pH value of the liquid reached approximately 6. After decantation, the resulting powder was washed 3 times with absolute ethanol and left to dry at room temperature for 3 days. Finally, the powder was dried in a vacuum oven (< 0.09 MPa) at 50°C for 24 hours to obtain Ti_3C_2 MXene.

Synthesis of TiO_2-Ti_3C_2 nanocomposite. Synthesis of TiO_2-Ti_3C_2 nanocomposite. Firstly, 150 mg of Ti_3C_2 was dispersed in 200 mL of ethanol and stirred at room temperature for 1 hour to obtain a homogeneous Ti_3C_2 suspension. 0.5 mL of 0.4 mM KCl (Aladdin, China) was added to the suspension and stirred for 20 minutes. Next, 1.0 mL of tetrabutyl titanate (Aladdin, China) was added to the mixture and stirred for 6 hours. At the end of the reaction, the gray precipitate was collected by centrifugation and sequentially washed 6 times with ethanol and 3 times with deionized water. After washing, the precipitate was dispersed in 60 mL of ethanol and stirred for 15 minutes. The resulting suspension was then loaded into a 100 mL Teflon-lined autoclave, which was sealed and heated in an MDS-8 microwave hydrothermal system at 180°C for 60 minutes. The TiO_2-Ti_3C_2 nanocomposite was collected, washed 3 times with ethanol and 3 times with pure water to remove ions and impurities, and then dried at 50°C to obtain the TiO_2-Ti_3C_2 nanocomposite.

The morphology and microstructure of the samples were observed by scanning electron microscopy (SEM) (Hitachi, Japan), and the nanoscale morphology and structure were observed by transmission electron microscopy (TEM) (Hitachi, Japan). Energy-dispersive X-ray spectroscopy (EDS) (Hitachi, Japan) was used to analyze the chemical composition of the elements in the samples, and high-angle annular dark-field scanning transmission electron microscopy (HAADF-STEM) (Hitachi, Japan) was used for high-resolution imaging of the samples to provide information on the structure and composition of the materials. X-ray powder diffraction (XRD) images were obtained using an X-ray diffractometer (Bruker, German). X-ray photoelectron spectroscopy (XPS) was performed on a K-Alpha 1063 instrument (Thermo Fisher Scientific, America).

Photothermal Performance Study of Ti_3C_2 and TiO_2-Ti_3C_2

An infrared thermal imaging camera (Fluke, America) was utilized to observe the real-time temperature changes during a predetermined time interval. A gradient concentration suspension of Ti_3C_2 and TiO_2-Ti_3C_2 (100 μL) was exposed to a 1064 nm laser (0.5 W/cm^2, 6 min) to observe the temperature evolution. The suspension of Ti_3C_2 and TiO_2-Ti_3C_2 (100 μL, 100 μg/mL) was irradiated with lasers (1064 nm) of varying power densities, while simultaneously monitoring the temperature changes in the suspension. For evaluating the photostability of Ti_3C_2 and TiO_2-Ti_3C_2, the water suspension of Ti_3C_2 and TiO_2-Ti_3C_2 (100 μL, 100 μg/mL) underwent repeated exposure to a 1064 nm laser (0.5 W/cm2, 6 min) followed by natural cooling. This process was repeated five times under identical conditions. To calculate the photothermal conversion efficiency of Ti_3C_2 and TiO_2-Ti_3C_2, the water suspension of TiO_2-Ti_3C_2 (100 μL, 100 μg/mL) was repeatedly irradiated with a 1064 nm laser (0.5 W/cm^2) until reaching a desired steady-state temperature. Subsequently, the laser was turned off, and the dynamic temperature was measured every 20 seconds during the cooling process.

Cell Culture and Reagents

Human normal colonic epithelial cells NCM-460 and human CRC cells SW480 were obtained from the American Type Culture Collection and cultured in DMEM (Gibco, America) containing 10% fetal bovine serum (Gibco, America) at 37°C in a humidified incubator with 5% CO_2.

CCK8

NCM-460 or SW480 cell suspensions at a density of 1×10^4 cells/mL were seeded into 96-well plates and cultured in an incubator, with 4 replicates per group at least. When the cell density reached approximately 70%, in a clean bench, the lid of the well plate was opened, and sterilized Ti_3C_2 or TiO_2-Ti_3C_2 was added to treat the cells. The cells were then irradiated with a NIR iodide laser (1064 nm, 0.5 W/cm^2) for 6 minutes (the laser treatment steps were the same for all in vitro experiments). After the laser irradiation, the cells were returned to a 37°C incubator. After 24 hours. The culture medium was then removed, and 100 μL of 10% CCK8 solution was added to each well. The plates were further incubated for 1.5 hours in the incubator, and the OD values of each well were measured at a wavelength of 450 nm to calculate cell viability. The experiment was performed in triplicate.

Transwell

Before inoculation, soak the 24-well plate and Transwell chambers in 1xPBS for 5 minutes to moisten the chambers. (For invasion experiments, add an additional step: Coat the chambers with 80μL of Matrigel gel and incubate at 37°C for 30 minutes to allow gelation.). After that, SW480 cell suspension at a density of 1×10^5 cells/mL was seeded into Transwell chambers, with 0.3 mL of cell suspension added to each chamber. 0.7 mL of complete medium containing 10% FBS was added to the lower 24-well plate. After 24–48 hours (Migration experiments were conducted for 24 hours of culture, while invasion experiments were conducted for 48 hours of culture), 1 mL of 4% paraformaldehyde solution was added to each well, and the plates were fixed at room temperature for 10 minutes. The fixative was removed, and the cells were washed with PBS. Next, 1 mL of 0.5% crystal violet solution was added to each well, and the cells were stained for 30 minutes. The cells were washed three times with PBS, air-dried, and observed under a microscope. The experiment was performed in triplicate.

Scratch Test

Start by using a marker pen and a ruler to mark even lines on the back of the 6-well plate, crossing each well with at least 5 lines. Prepare a SW480 cell suspension at a density of 1×105 cells/mL and seed it into the 6-well plate. When the cell density reaches approximately 70%, use a 200 μL pipette tip to create scratches along the bottom lines of the 6-well plate. Then, add sterilized Ti_3C_2 or TiO_2-Ti_3C_2 (100 μg/mL) to treat the cells. Subsequently, irradiate the cells with NIR (1064 nm, 0.5 W/cm^2) for 6 minutes. After the laser irradiation, return the cells to a 37°C incubator. After 24 hours, wash the cells with PBS, remove the back lines on the 6-well plate using 75% ethanol, and add serum-free medium before capturing pictures. The experiment was performed in triplicate.

Flow Cytometry

A suspension of SW480 cell at a density of 1×10^5 cells/mL was prepared and seeded into the 6-well plate. When the cell density reached approximately 70%, sterilized Ti_3C_2 or TiO_2-Ti_3C_2 (100 μg/mL) was added to treat the cells, then the cells were then irradiated with NIR (1064 nm, 0.5 W/cm^2) for 6 minutes. After the laser irradiation, the cells were returned to a 37°C incubator. After 24 hours, the cells were collected and resuspended in 1× binding buffer at a concentration of 1×10^6 cells/mL. Then, 100 μL of the solution (1×10^5 cells) was transferred to a 5 mL culture tube. FITC Annexin V (BD Pharmingen, America) and PI (BD Pharmingen, America) at a volume of 5μL each were added to the tube, mixed thoroughly, and incubated in the dark at 25°C for 15 minutes. Subsequently, 400 μL of 1x binding buffer was added to each tube, and the samples were immediately analyzed using a flow cytometer (Beckman Coulter). All experiments were performed in triplicate at least.

Animal Models

Twenty male BALB/c. Nude mice, aged 4–5 weeks, were randomly divided into 4 groups: PBS, Ti_3C_2, Ti_3C_2+NIR, and TiO_2-Ti_3C_2+NIR. A suspension of SW480 cell with a density of 2×10^7cells/mL was prepared. Each mouse was subcutaneously injected with 100 μL of the cell suspension. After 7 days, when the tumors reached the size of 50–100 mm^3, Ti_3C_2 or TiO_2-Ti_3C_2 was injected into the tumor (5 mg/kg, once every 4 days for a total of 6 injections), and combined with light treatment (1064 nm, 6 minutes). After 24 days, the mice were sacrificed, and tissues were collected for analysis.

Hematoxylin and Eosin Staining (H&E Staining)

After dehydration and embedding, the tissues were sliced into sections with a thickness of 5 μm using a microtome. The complete tissue sections were mounted on regular glass slides, subjected to hematoxylin and eosin staining, and ultimately sealed with neutral resin. The samples were observed under an optical microscope.

Immunohistochemistry

4 μm-thick sections were obtained from paraffin-embedded tissues using a microtome. Subsequently, the complete tissue sections were mounted on adhesive glass slides, deparaffinized, and underwent antigen retrieval through microwave treatment in citrate buffer for 10 minutes. Following the cooling step, the samples were blocked for 1 hour and then incubated overnight at 4°C with Ki67 antibody (Cell Signaling Technology, 9449T). The next day, the samples were incubated with SignalStain® Boost Detection Reagent (HRP, Mouse #8125) at room temperature for 30 minutes, washed, and incubated with SignalStain® DAB Substrate Kit (Cell Signaling Technology, 8059). Finally, the samples were observed under a microscope.

Terminal Deoxynucleotidyl Transferase dUTP Nick End Labeling (TUNEL) Staining

Sections with a thickness of 4 μm were prepared from paraffin-embedded tissues using a microtome. The resulting tissue sections were mounted on adhesive glass slides, followed by deparaffinization and treatment with 20 μg/mL proteinase K (without DNase) at room temperature for 15–30 minutes. Then, the samples were washed three times with PBS and incubated with TUNEL detection solution (Beyotime, C1086) at 37°C in the dark for 60 minutes. After three additional washes with PBS, the samples were sealed with an anti-fluorescence quenching agent and observed under a fluorescence microscope.

Statistical Analysis

All analyses were performed using the GraphPad Prism 8 Software. A one-way ANOVA was used to analyze statistical differences. All data are presented as the mean with standard deviation (SD) from at least three individual experiments. $P<0.05$ was considered statistically significant.

Results

Structural Characterization of TiO_2-Ti_3C_2 Nanocomposites

As shown in Figure 1A and B, the TiO_2-Ti_3C_2 nanocomposite exhibits a sheet-like structure. Furthermore, the SAED diffraction pattern (Figure 1C) indicates that the crystal structure is highly ordered and well-defined, with good

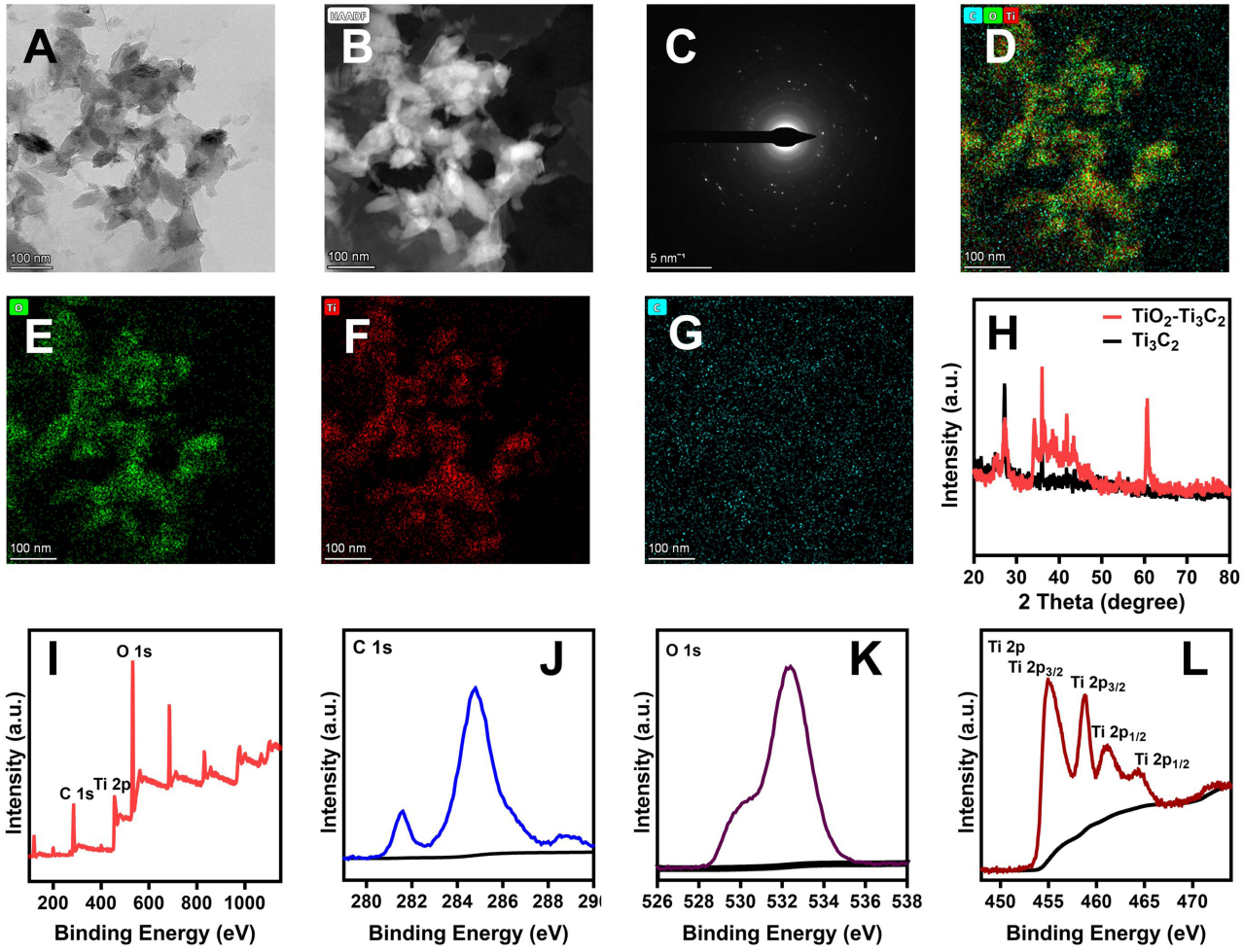

Figure 1 Structure characterization of Ti_3C_2 and TiO_2-Ti_3C_2. (**A**) TEM images of TiO_2-Ti_3C_2. (**B**) High-resolution TEM images of TiO_2-Ti_3C_2. (**C**) SAED images of TiO_2-Ti_3C_2. (**D–G**) HAADF-STEM-EDS elemental mappings of Ti, C, O component of TiO_2-Ti_3C_2. (**H**) XRD pattern of Ti_3C_2 and TiO_2-Ti_3C_2. (**I**) Full XPS spectra of TiO_2-Ti_3C_2. XPS spectra of (**J**) C 1s regions, (**K**) O 1s regions, and (**L**) Ti 2p regions.

crystallinity. The STEM-EDS elemental distribution mapping (Figure 1D–G) prepared according to the sample shows that C, O, and Ti coexist in the prepared nanocomposite, further confirming the elemental composition of TiO_2-Ti_3C_2. The XRD peaks of Ti_3C_2 and TiO_2-Ti_3C_2 are shown in Figure 1H, which exhibit both the characteristic peaks of Ti_3C_2 and the diffraction peaks of TiO_2 (TiO_2: JCPDS no. 21–1272).In addition, as shown in Figure 1I–L, the peak at 284.8 eV corresponds to the binding energy of C 1s,[24] Ti 2p 2/3 and Ti 2p 1/2 the peak at 532 eV belongs to the typical peak of O 1s, and the peaks at 454.8 and 459, 461.3 and 464.5 eV belong to Ti 2p 2/3 and Ti 2p 1/2, respectively.[24,25] These results collectively indicate the successful preparation of the TiO_2-Ti_3C_2 nanocomposite.

The Photothermal Properties of Ti_3C_2 and TiO_2-Ti_3C_2

Real-time monitoring of temperature changes in Ti_3C_2 and TiO_2-Ti_3C_2 was performed using a FLUKE thermal imaging camera. In Figure 2A and D, the temperature of Ti_3C_2 and TiO_2-Ti_3C_2 increased in a concentration-dependent manner (0–200 μg/mL) and a power-dependent manner (0.25–1.0 W/cm^2). At a concentration of 100 μg/mL and laser irradiation conditions of 0.5 W/cm^2, 1064 nm, and 6 minutes, the temperature of Ti_3C_2 reached 35°C (Figure 2A and B), while the temperature of TiO_2-Ti_3C_2 reached 60°C (Figure 2D and E), indicating that TiO_2-Ti_3C_2 has good absorption in the NIR-II region and can efficiently convert light energy into heat. To further study the photothermal properties of TiO_2-Ti_3C_2, photothermal stability, and conversion efficiency were measured. As shown in Figure 2E, after five cycles of heating and cooling, the photothermal effect of TiO_2-Ti_3C_2 remained unchanged, indicating its good photothermal stability, which is

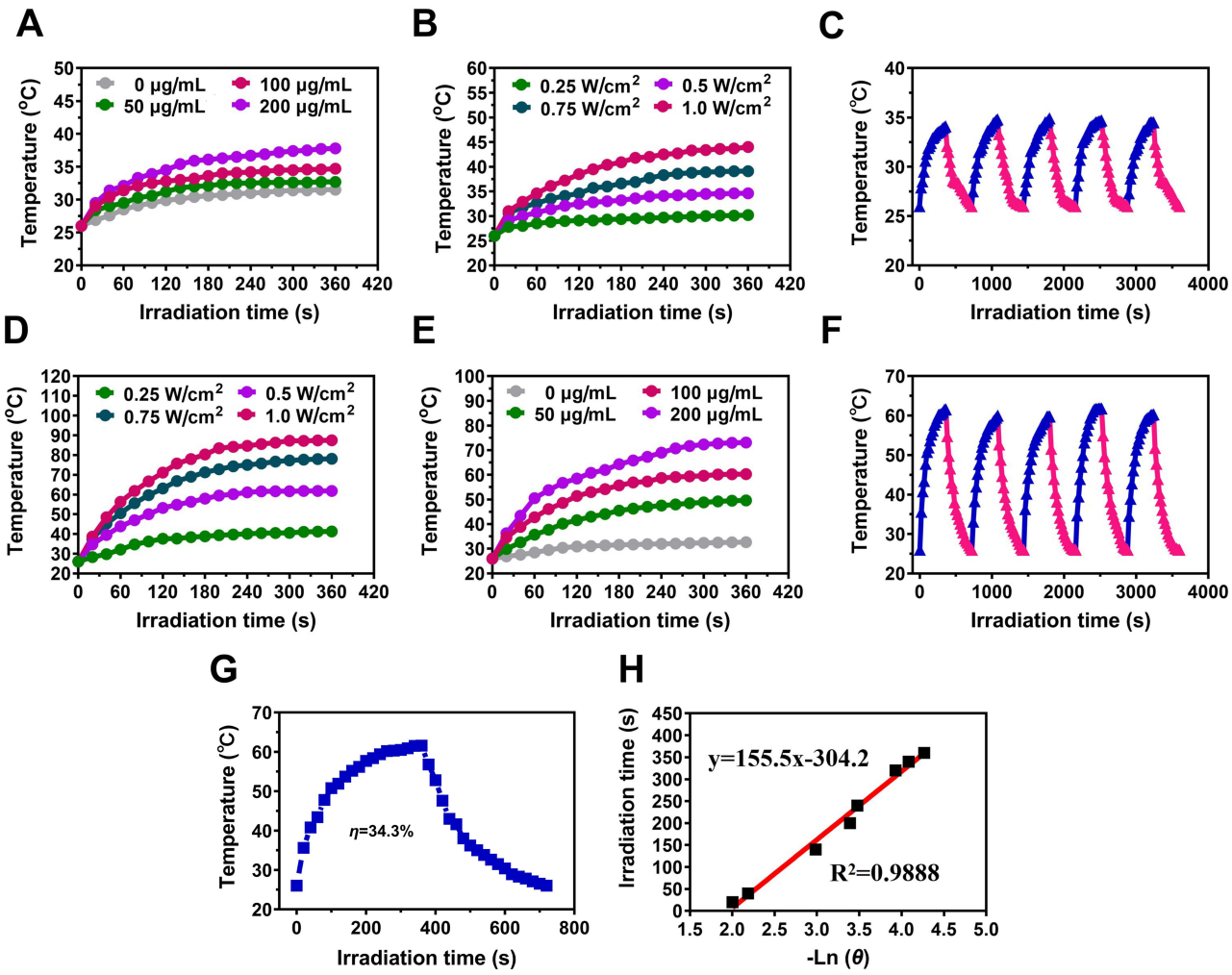

Figure 2 The photothermal properties of Ti_3C_2 and TiO_2-Ti_3C_2 are shown in (**A**) Temperature change curves of Ti_3C_2 at different concentrations under laser irradiation (1064 nm, 0.5 W/cm^2) for 6 minutes; (**B**) Temperature change curve of Ti_3C_2 (100 μg/mL) under different power levels of 1064 nm laser irradiation; (**C**) Photothermal stability measurement of Ti_3C_2 under five cycles of on/off NIR laser (0.5 W/cm^2); (**D**) Temperature change curves of TiO_2-Ti_3C_2 at different concentrations under laser irradiation (1064 nm, 0.5 W/cm^2) for 6 minutes; (**E**) Temperature change curve of TiO_2-Ti_3C_2 (100 μg/mL) under different power levels of 1064 nm laser irradiation; (**F**) Photothermal stability measurement of TiO_2-Ti_3C_2 under five cycles of on/off NIR laser (0.5 W/cm^2); (**G**) Temperature-time curve of TiO_2-Ti_3C_2 reaching steady-state temperature and cooling naturally; (**H**) Linear fitting plot of time during cooling period and −lnθ.

important for its application in PTT. The photothermal conversion efficiency (η) was calculated using the method provided to quantify the photothermal effect.[26] The η value of TiO_2-Ti_3C_2 was determined to be approximately 34.3% (Figure 2G and H). It can be seen that after encapsulation with TiO_2, TiO_2-Ti_3C_2 exhibits superior absorption capacity in the NIR-II region, excellent photothermal performance, strong stability, and high photothermal conversion efficiency. Therefore, it is a nanomaterial with great potential for PTT. In addition, we determined that the optimal concentration of TiO_2-Ti_3C_2 composite material is 100 μg/mL, the optimal laser irradiation conditions are at a wavelength of 1064 nm, with an intensity of 0.5 W/cm^2 and continuous irradiation for 6 minutes.

In vitro Cytotoxicity of TiO_2-Ti_3C_2 Against Colorectal Cancer Cells

TiO_2-Ti_3C_2 exhibited excellent photothermal activity, suggesting its potential for killing colorectal cancer cells through photothermal conversion. CCK8 assays showed that both Ti_3C_2 and TiO_2-Ti_3C_2 at various concentrations (0, 2, 4, 8, 16, 32, 64, 128, and 256 μg/mL) had no significant cytotoxicity against NCM-460 cells after 24 hours of treatment (Figure 3A), indicating their negligible toxicity to normal cells. Based on this, we further investigated the effect of TiO_2-Ti_3C_2's photothermal properties on colorectal cancer cells by setting Control, TiO_2-Ti_3C_2, Ti_3C_2+NIR, and TiO_2-Ti_3C_2+NIR

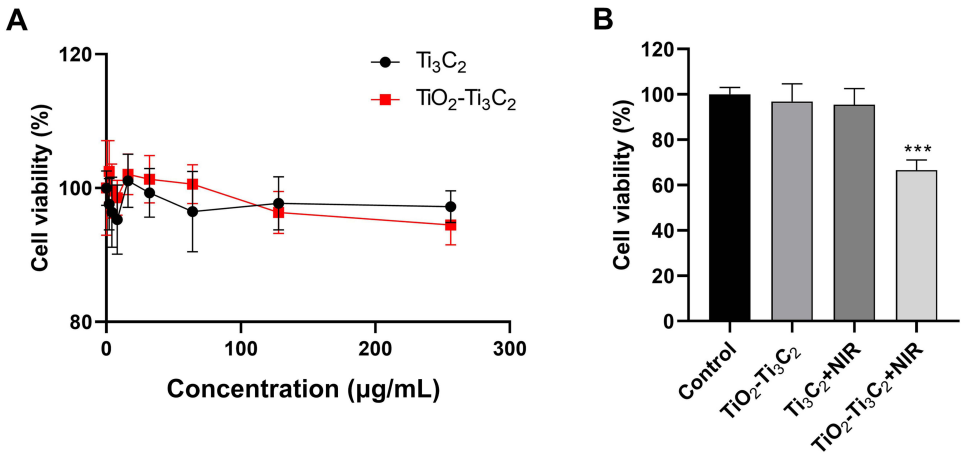

Figure 3 The impact of TiO_2-Ti_3C_2 on the viability of normal colonic epithelial cells and CRC cells. (**A**) CCK8 assay for NCM-460 cell viability; (**B**) CCK8 assay for SW480 cell viability, ***P<0.001.

groups. CCK8 assays showed that the viability of SW480 cells was significantly reduced in the TiO_2-Ti_3C_2+NIR group (100 μg/mL TiO_2-Ti_3C_2 and NIR at 1064 nm, 0.5 W/cm^2, 6 min) compared to the other groups, while no significant changes were observed in the TiO_2-Ti_3C_2 (100 μg/mL) and Ti_3C_2+NIR groups (100 μg/mL) (Figure 3B).

Transwell assays (Figure 4A) demonstrated that 100 μg/mL TiO_2-Ti_3C_2 without NIR irradiation and Ti_3C_2 after NIR irradiation had no significant effect on the invasion and migration of SW480 cells; in contrast, TiO_2-Ti_3C_2 after NIR irradiation significantly inhibited the invasion and migration of SW480 cells. Scratch assays (Figure 4B) also showed that only TiO_2-Ti_3C_2 after NIR irradiation could inhibit the migration and proliferation of colorectal cancer cells. Furthermore, flow cytometry confirmed the pro-apoptotic effect of TiO_2-Ti_3C_2 and NIR on colorectal cancer cells. As shown in Figure 4C, no significant apoptosis of SW480 cells was observed in the Ti_3C_2 and TiO_2-Ti_3C_2 groups (without NIR irradiation), whereas TiO_2-Ti_3C_2 after NIR irradiation significantly induced apoptosis of SW480 cells. In conclusion, due to its excellent photothermal activity, TiO_2-Ti_3C_2 nanocomposites can inhibit the invasion, migration, and proliferation of colorectal cancer cells and induce apoptosis.

In vivo Inhibitory Effect of TiO_2-Ti_3C_2 on CRC

To further investigate the effect of TiO_2-Ti_3C_2 on mice tumors, we established a subcutaneous SW480 xenograft model and administered PBS, TiO_2-Ti_3C_2, Ti_3C_2+NIR, and TiO_2-Ti_3C_2+NIR treatments. As shown in Figure 5A, there was no significant difference in tumor volume or weight between the PBS, TiO_2-Ti_3C_2, and Ti_3C_2+NIR groups, while the combination of TiO_2-Ti_3C_2 and NIR led to a significant reduction in tumor volume and weight, indicating the inhibition of tumor growth. TiO_2-Ti_3C_2 nanospheres combined with NIR treatment had a certain degree of tumor regression effect. Ki67 protein is highly expressed in cancer cells and is a commonly used tumor marker to evaluate cell proliferation activity. It exists in the mitotic phase of the cell cycle, as well as in the early stages of G1, S, and G2, but not in the G0 phase.[27] Subsequently, we performed HE staining and IHC on tumor tissue. TiO_2-Ti_3C_2+NIR treatment inhibited tumor cell proliferation, as evidenced by the local necrosis of tumor tissue (indicated by black arrows) and weak Ki67 staining in tumor tissue (Figure 5B). TUNEL results further showed that TiO_2-Ti_3C_2+NIR treatment increased tumor cell apoptosis, as evidenced by stronger TUNEL fluorescence staining in tumor tissue (Figure 5C). These results suggest that TiO_2-Ti_3C_2 nanocomposites have excellent photothermal activity in vivo and can target tumor tissue to inhibit tumor cell proliferation and induce tumor cell apoptosis, thereby inhibiting the development of CRC.

However, while exploring the inhibitory effect of TiO_2-Ti_3C_2 nanospheres combined with NIR treatment on tumors, it is also important to pay attention to their biocompatibility. Therefore, we performed HE staining on the major organs of mice, including the heart, liver, spleen, lungs, and kidneys, and found no significant pathological changes in the tissue morphology of major organs, indicating that Ti_3C_2 and TiO_2-Ti_3C_2 nanospheres have good biocompatibility (Figure 6).

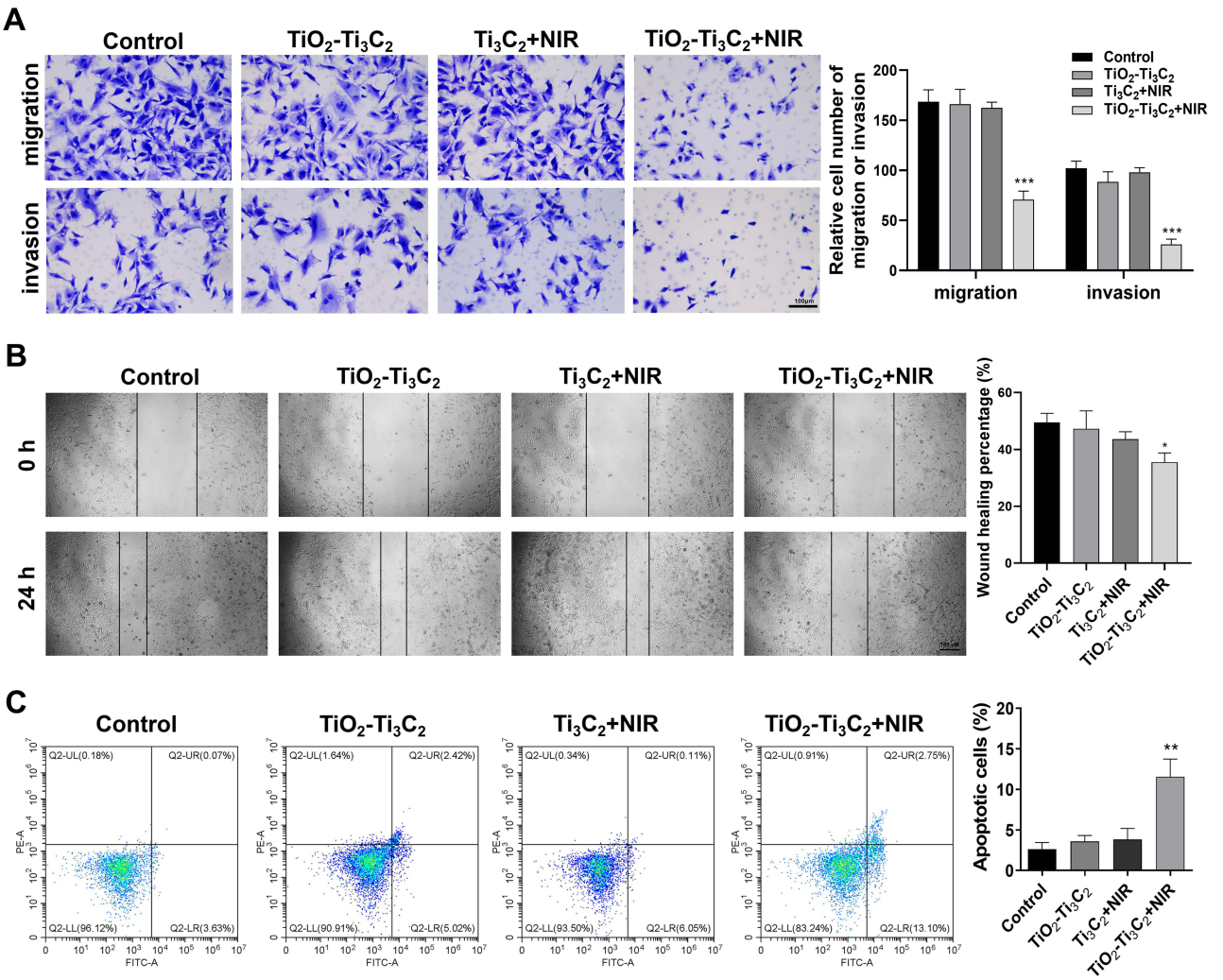

Figure 4 The effects of TiO_2-Ti_3C_2 on the migration, invasion, and apoptosis of CRC cells. (**A**) Transwell assay for SW480 cell invasion and migration; (**B**) Scratch assay for SW480 cell proliferation and migration; (**C**) Flow cytometry analysis of cell apoptosis. *P<0.05, **P<0.01, ***P<0.001.

Discussion

The high incidence rate, low survival rate, and adverse reactions associated with traditional treatments such as surgery and chemotherapy present significant challenges in the treatment of CRC. There is an urgent need to find effective and low-risk treatment methods to address these issues.[1,4–6] PTT provides a promising solution by avoiding surgical risks, reducing chemotherapy-related adverse reactions, and significantly lowering treatment costs.[10] This approach involves direct irradiation of the target organ with NIR light, offering the potential to revolutionize traditional cancer treatment methods. Ti_3C_2, with its excellent NIR absorption and photothermal performance, emerges as a promising candidate for photothermal conversion agents.[16] Additionally, TiO_2 has gained widespread usage in cancer diagnosis and treatment due to its low toxicity, good biocompatibility, and stability.[28,29] Therefore, in our study, we employed a TiO_2-Ti_3C_2 composite material to further enhance the biocompatibility, stability, and photothermal conversion efficiency of Ti_3C_2. Our findings demonstrate that TiO_2-Ti_3C_2 exhibits not only excellent photothermal conversion efficiency in the NIR-II region but also a significant inhibitory effect on CRC while demonstrating low toxicity to normal cell tissue.

In PTT, the photothermal agent's characteristics, such as high light absorption at the processing wavelength, high photothermal conversion efficiency, and photostability, play crucial roles. To begin, we confirmed the TiO_2-Ti_3C_2 nanocomposite as the material used in our study through a thorough examination of its morphology, elemental composition, and chemical composition. Subsequently, we conducted a detailed investigation of the photothermal

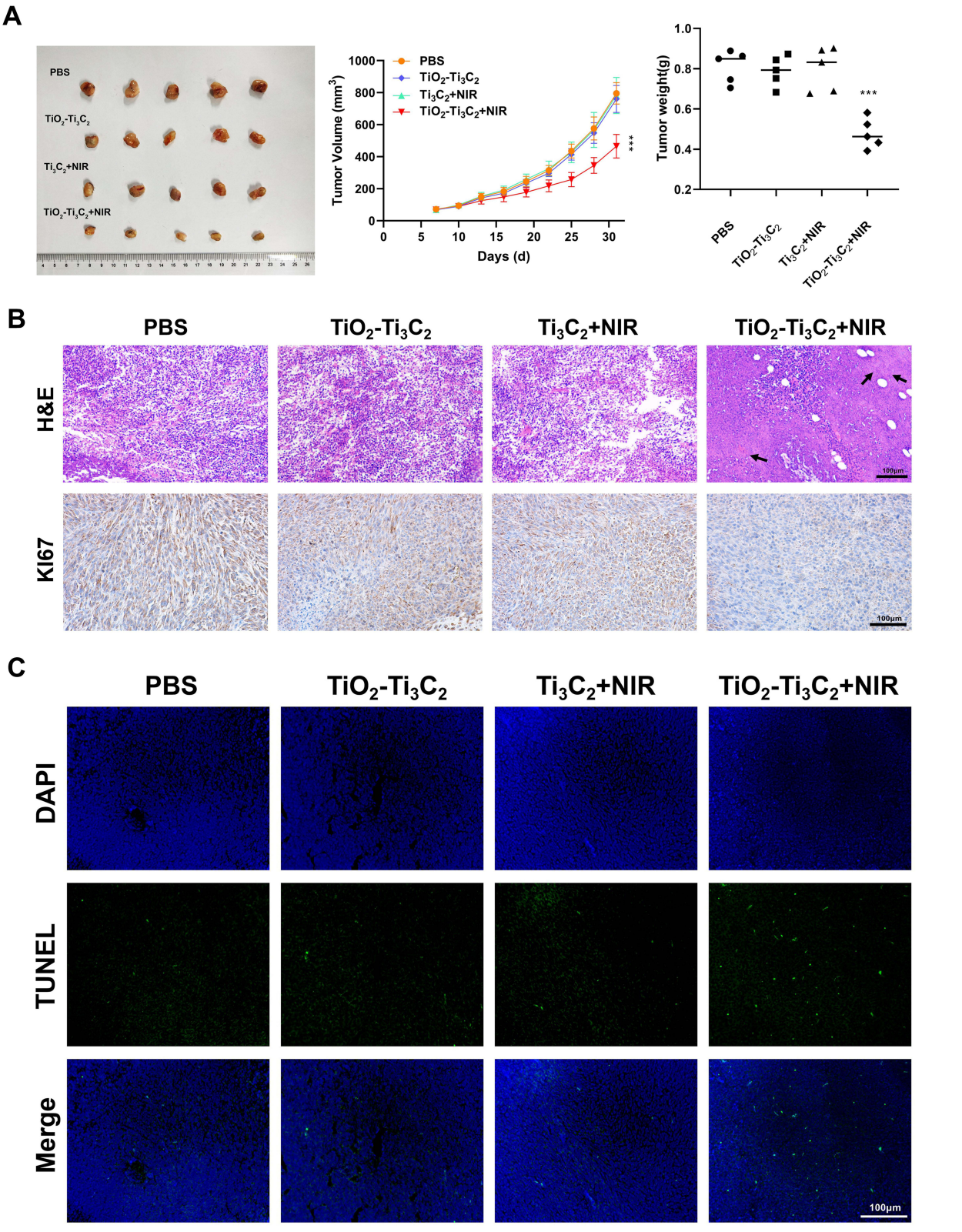

Figure 5 In vivo inhibitory effect of TiO_2-Ti_3C_2 on colorectal cancer. (**A**) Changes in mice tumors volume and weight; (**B**) IHC detection of the tumor marker Ki67 and HE staining to observe the morphological changes in the tumor; (**C**) TUNEL staining to detect tumor cell apoptosis. ***P<0.001.

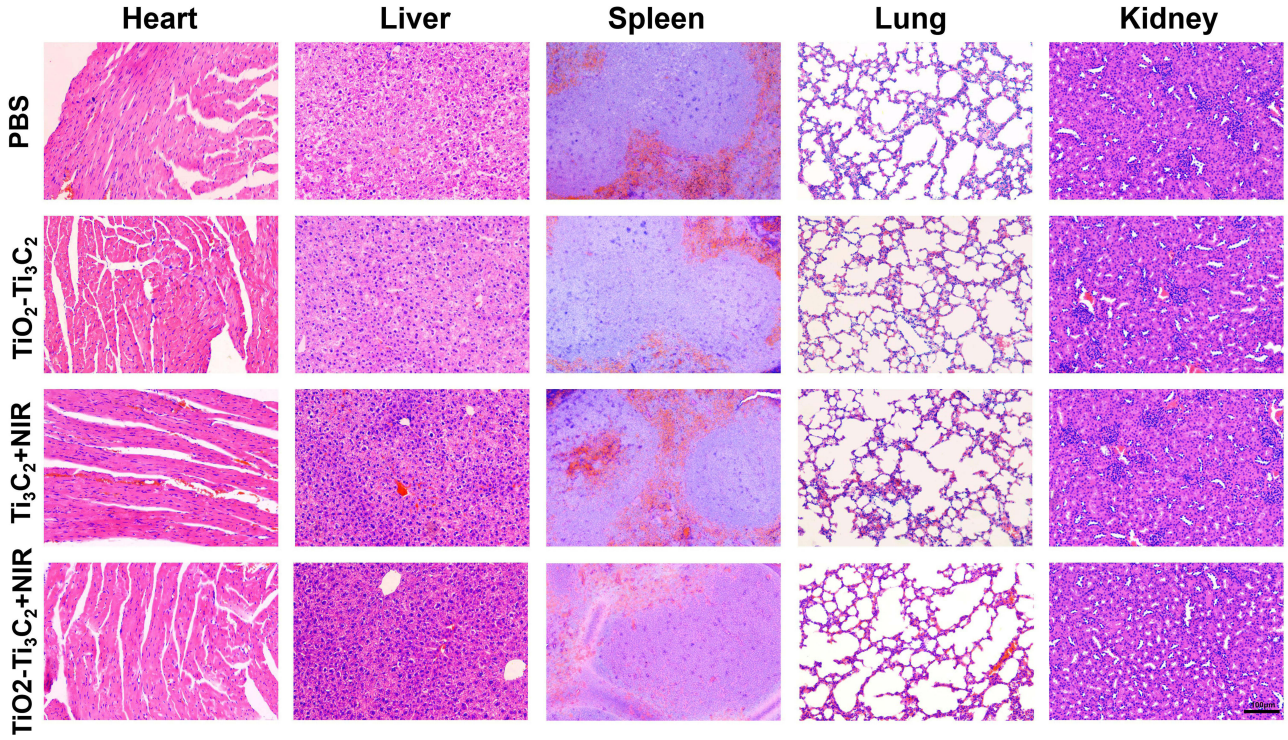

Figure 6 The biocompatibility of TiO_2-Ti_3C_2. HE staining to assess the morphological changes in the heart, liver, spleen, lungs, and kidneys of mice.

properties of TiO_2-Ti_3C_2. In PPT, when the photothermal agent is irradiated with light of a specific wavelength, it transitions from the ground-state singlet state to the excited singlet state, absorbs photon energy, and returns to the ground state through collisions with surrounding molecules mediated by the excited photothermal agent, leading to an increase in the temperature of the surrounding microenvironment.[13] When the tissue temperature exceeds 60°C, cells die almost instantly due to protein denaturation and membrane damage.[13,30] In our study, when the laser irradiation conditions were set at 1064 nm, 0.5 W/cm^2 for 6 min, the temperature of 100 μg/mL TiO_2-Ti_3C_2 reached 60°C, which is sufficient for the instant killing of tumor cells. The η value of TiO_2-Ti_3C_2 in the NIR-II (1064 nm) region reaches 34.3%, which is superior or even comparable to many previously reported photothermal nanoagents.[16,31–33] In addition, after five cycles of heating and cooling, the photothermal effect of TiO_2-Ti_3C_2 remained stable These results indicate that the TiO_2-Ti_3C_2 nanocomposite exhibits good absorption in the NIR-II region, has efficient photothermal conversion ability, and has stable photothermal performance.

Based on our previous study of the photothermal activity of TiO_2-Ti_3C_2, we established the laser processing conditions for subsequent in vitro and in vivo studies to be 1064 nm wavelength, 0.5 W/cm^2, and continuous irradiation for 6 min. An earlier in vitro study showed that Ti_3C_2 MXene had no significant inhibitory effect on human normal epidermal cells (such as Hacat cells) but had a significant inhibitory effect on human malignant melanoma cells (such as A357 cells). When the concentration of Ti_3C_2 MXene reached 125 μg/mL, the viability of both human normal lung cells (such as MRC-5 cells) and human lung cancer cells (such as A549 cells) was significantly inhibited.[34]

Our CCK8 results showed that both Ti_3C_2 and TiO_2-Ti_3C_2 had no significant toxicity to human normal colon cells in vitro, and TiO_2-Ti_3C_2 and Ti_3C_2 (with NIR irradiation) had no significant toxicity to human colorectal cancer cells. However, after irradiation with a 1064 nm laser, TiO_2-Ti_3C_2 showed a significant inhibitory effect on human colorectal cancer cells. We attribute the differences in results to the varying sensitivity of different cells to nanoparticles and the concentration of the materials. In addition, other studies have demonstrated that Ti_3C_2 exhibits excellent conversion efficiency when irradiated with an 808 nm laser, leading to effective cancer cell killing and tumor tissue destruction through photothermal/photodynamic/chemical synergistic therapy.[35] However, in our investigation, Ti_3C_2 combined with NIR irradiation did not exhibit a significant inhibitory effect on tumor cells, possibly due to its limited absorption ability

at a wavelength of 1064 nm and a resulting temperature increase of only 35°C after photothermal conversion, which was insufficient to induce cell damage. Transwell and scratch experiments showed that after irradiation with a 1064 nm laser, TiO_2-Ti_3C_2 significantly inhibited the invasion and migration of SW480 cells. These data indicate that TiO_2-Ti_3C_2 plays a role in inhibiting the invasion and migration of colorectal cancer cells and inducing their apoptosis by absorbing light energy and converting it into heat. However, further research is necessary to elucidate the underlying molecular mechanism of the TiO_2-Ti_3C_2+NIR effect.

In our in vivo study, we found that TiO_2-Ti_3C_2 combined with NIR treatment significantly inhibited tumor volume and growth. However, for anti-tumor drugs, biocompatibility is also an important aspect that needs to be considered. It has been reported that Ti_3C_2@TiO_2-x-PEG composite materials exhibit good biocompatibility and have no significant effect on tissue morphology in the heart, liver, spleen, lungs, and kidneys of mice while inhibiting tumor growth.[34] Similar results were obtained in our study. By observing the HE staining results of various organs (heart, liver, spleen, lungs, and kidneys) in each group, we found no significant difference between the treatment group and the control group, indicating that the materials had no significant toxic side effects on other organs. Further studies showed that after TiO_2-Ti_3C_2+NIR treatment, localized necrosis of tumor tissue occurred, Ki67 expression was decreased, and tumor cell apoptosis was significantly increased, indicating that TiO_2-Ti_3C_2+NIR not only has good biocompatibility but also can efficiently target tumor tissue, inhibit tumor proliferation, and induce tumor tissue apoptosis and necrosis.

Conclusion

In conclusion, our study has provided a comprehensive understanding of the photothermal activity of TiO_2-Ti_3C_2 and demonstrated its photothermal effects both in vitro and in vivo. When exposed to a 1064 nm laser (0.5 W/cm^2, 6 min), TiO_2-Ti_3C_2 exhibited remarkable photothermal conversion efficiency, specifically targeted tumor tissue, and effectively inhibited tumor cell invasion, migration, and proliferation. Furthermore, it induced apoptosis in tumor cells, ultimately impeding the progression of CRC. The TiO_2-Ti_3C_2 composite shows promise as a NIR-II absorbing material and holds great potential for application in PTT for CRC.

Abbreviations

CRC, colorectal cancer; PTT, photothermal therapy; NIR-I, near-infrared region I; NIR-II, near-infrared region II; SEM, scanning electron microscopy; TEM, transmission electron microscopy; EDS, Energy-dispersive X-ray spectroscopy; HAADF-STEM, high-angle annular dark-field scanning transmission electron microscopy; XRD, X-ray powder diffraction; XPS, X-ray photoelectron spectroscopy; SD, standard deviation.

Data Sharing Statement

The datasets used and/or analyzed in the study are available from the corresponding author on reasonable request.

Ethics Approval

All experimental protocols were reviewed and approved by the Wenzhou Medical University Experimental Animal Ethics Committee (wydw2023-0507).

All animal research was conducted in accordance with the standards outlined in the 8th edition of "Guide for the Care and Use of Laboratory Animals" published by the National Academy of Sciences, National Academies Press, Washington, D.C.

Acknowledgments

This study was supported by the National Natural Science Foundation of China (81902891). Graphical abstract was created with Biorender.com.

Disclosure

The authors report no conflicts of interest in this work.

References

1. Miller KD, Nogueira L, Devasia T, et al. Cancer treatment and survivorship statistics, 2022. *CA Cancer J Clin*. 2022;72(5):409–436. doi:10.3322/caac.21731
2. Sung H, Ferlay J, Siegel RL, et al. Global cancer statistics 2020: GLOBOCAN estimates of incidence and mortality worldwide for 36 cancers in 185 countries. *CA Cancer J Clin*. 2021;71(3):209–249. doi:10.3322/caac.21660
3. Siegel RL, Miller KD, Goding Sauer A, et al. Colorectal cancer statistics, 2020. *CA Cancer J Clin*. 2020;70(3):145–164. doi:10.3322/caac.21601
4. Schover LR, van der Kaaij M, van Dorst E, Creutzberg C, Huyghe E, Kiserud CE. Sexual dysfunction and infertility as late effects of cancer treatment. *EJC Suppl*. 2014;12(1):41–53. doi:10.1016/j.ejcsup.2014.03.004
5. Den Oudsten BL, Traa MJ, Thong MS, et al. Higher prevalence of sexual dysfunction in colon and rectal cancer survivors compared with the normative population: a population-based study. *Eur J Cancer*. 2012;48(17):3161–3170. doi:10.1016/j.ejca.2012.04.004
6. Liu L, Herrinton LJ, Hornbrook MC, Wendel CS, Grant M, Krouse RS. Early and late complications among long-term colorectal cancer survivors with ostomy or anastomosis. *Dis Colon Rectum*. 2010;53(2):200–212. doi:10.1007/DCR.0b013e3181bdc408
7. Sun V, Grant M, Wendel CS, et al. Sexual function and health-related quality of life in long-term rectal cancer survivors. *J Sex Med*. 2016;13(7):1071–1079. doi:10.1016/j.jsxm.2016.05.005
8. Lee SY, Shieh MJ. Platinum(II) drug-loaded gold nanoshells for chemo-photothermal therapy in colorectal cancer. *ACS Appl Mater Interfaces*. 2020;12(4):4254–4264. doi:10.1021/acsami.9b18855
9. Wang S, Song Y, Cao K, et al. Photothermal therapy mediated by gold nanocages composed of anti-PDL1 and galunisertib for improved synergistic immunotherapy in colorectal cancer. *Acta Biomater*. 2021;134:621–632. doi:10.1016/j.actbio.2021.07.051
10. Hao M, Kong C, Jiang C, et al. Polydopamine-coated Au-Ag nanoparticle-guided photothermal colorectal cancer therapy through multiple cell death pathways. *Acta Biomater*. 2019;83:414–424. doi:10.1016/j.actbio.2018.10.032
11. Hu K, Xie L, Zhang Y, et al. Marriage of black phosphorus and Cu(2+) as effective photothermal agents for PET-guided combination cancer therapy. *Nat Commun*. 2020;11(1):2778. doi:10.1038/s41467-020-16513-0
12. Tang B, Li WL, Chang Y, et al. A supramolecular radical dimer: high-efficiency nir-ii photothermal conversion and therapy. *Angew Chem Int Ed Engl*. 2019;58(43):15526–15531. doi:10.1002/anie.201910257
13. Li X, Lovell JF, Yoon J, Chen X. Clinical development and potential of photothermal and photodynamic therapies for cancer. *Nat Rev Clin Oncol*. 2020;17(11):657–674. doi:10.1038/s41571-020-0410-2
14. Xu X, Wang S, Wu H, Liu Y, Xu F, Zhao J. A multimodal antimicrobial platform based on MXene for treatment of wound infection. *Colloids Surf B Biointerfaces*. 2021;207:111979. doi:10.1016/j.colsurfb.2021.111979
15. Zhang Y, Zhang S, Zhang Z, et al. Recent progress on NIR-II photothermal therapy. *Front Chem*. 2021;9:728066. doi:10.3389/fchem.2021.728066
16. Zhang DY, Liu H, Younis MR, et al. In-situ TiO(2-x) decoration of titanium carbide MXene for photo/sono-responsive antitumor theranostics. *J Nanobiotechnology*. 2022;20(1):53. doi:10.1186/s12951-022-01253-8
17. Zhang X, Zhao J, Xie P, Wang S. Biomedical applications of electrets: recent advance and future perspectives. *J Funct Biomater*. 2023;14(6):320.
18. Wang F, Yang C, Duan M, Tang Y, Zhu J. TiO2 nanoparticle modified organ-like Ti3C2 MXene nanocomposite encapsulating hemoglobin for a mediator-free biosensor with excellent performances. *Biosens Bioelectron*. 2015;74:1022–1028. doi:10.1016/j.bios.2015.08.004
19. Xu C, He Y, Li Z, Ahmad Nor Y, Ye Q. Nanoengineered hollow mesoporous silica nanoparticles for the delivery of antimicrobial proteins into biofilms. *J Mater Chem B*. 2018;6(13):1899–1902. doi:10.1039/c7tb03201c
20. Tasia W, Lei C, Cao Y, Ye Q, He Y, Xu C. Enhanced eradication of bacterial biofilms with DNase I-loaded silver-doped mesoporous silica nanoparticles. *Nanoscale*. 2020;12(4):2328–2332. doi:10.1039/c9nr08467c
21. Na KJ, Park GC. Improved treatment of photothermal cancer by coating TiO2 on porous silicon. *J Nanosci Nanotechnol*. 2016;16(2):1375–1378. doi:10.1166/jnn.2016.12024
22. Chang X, Wu Q, Wu Y, et al. Multifunctional Au modified Ti(3)C(2)-MXene for photothermal/enzyme dynamic/immune synergistic therapy. *Nano Lett*. 2022;22(20):8321–8330. doi:10.1021/acs.nanolett.2c03260
23. Guo Y, Wang H, Feng X, et al. 3D MXene microspheres with honeycomb architecture for tumor photothermal/photodynamic/chemo combination therapy. *Nanotechnology*. 2021;32(19):195701. doi:10.1088/1361-6528/abe153
24. Peng C, Yang X, Li Y, Yu H, Wang H, Peng F. Hybrids of two-dimensional Ti3C2 and TiO2 exposing 001 facets toward enhanced photocatalytic activity. *ACS Appl Mater Interfaces*. 2016;8(9):6051–6060. doi:10.1021/acsami.5b11973
25. Li L, Jiang G, An C, et al. Hierarchical Ti(3)C(2)@TiO(2) MXene hybrids with tunable interlayer distance for highly durable lithium-ion batteries. *Nanoscale*. 2020;12(18):10369–10379. doi:10.1039/d0nr01222j
26. Liu J, Zheng X, Yan L, et al. Bismuth sulfide nanorods as a precision nanomedicine for in vivo multimodal imaging-guided photothermal therapy of tumor. *ACS Nano*. 2015;9(1):696–707. doi:10.1021/nn506137n
27. Yang C, Zhang J, Ding M, et al. Ki67 targeted strategies for cancer therapy. *Clin Transl Oncol*. 2018;20(5):570–575. doi:10.1007/s12094-017-1774-3
28. Xu W, Lin Q, Yin Y, et al. A Review on cancer therapy based on the photothermal effect of gold nanorod. *Curr Pharm Des*. 2019;25(46):4836–4847. doi:10.2174/1381612825666191216150052
29. Tonelli FMP, Tonelli FCP, Cordeiro HG. TiO2 nanoparticles in cancer therapy as nanocarriers in paclitaxel's delivery and nanosensitizers in phototherapies and/or sonodynamic therapy. *Curr Pharm Biotechnol*. 2023. doi:10.2174/1389201024666230518124829
30. Knavel EM, Brace CL. Tumor ablation: common modalities and general practices. *Tech Vasc Interv Radiol*. 2013;16(4):192–200. doi:10.1053/j.tvir.2013.08.002
31. Hessel CM, Pattani VP, Rasch M, et al. Copper selenide nanocrystals for photothermal therapy. *Nano Lett*. 2011;11(6):2560–2566. doi:10.1021/nl201400z
32. Yang T, Tang Y, Liu L, et al. Size-dependent Ag(2)S nanodots for second near-infrared fluorescence/photoacoustics imaging and simultaneous photothermal therapy. *ACS Nano*. 2017;11(2):1848–1857. doi:10.1021/acsnano.6b07866
33. Rizwan M, Roy VAL, Abbasi R, et al. Novel 2D mxene cobalt ferrite (CoF@Ti(3)C(2)) composite: a promising photothermal anticancer in vitro study. *ACS Biomater Sci Eng*. 2023. doi:10.1021/acsbiomaterials.3c01328
34. Jastrzebska AM, Szuplewska A, Wojciechowski T, et al. In vitro studies on cytotoxicity of delaminated Ti(3)C(2) MXene. *J Hazard Mater*. 2017;339:1–8. doi:10.1016/j.jhazmat.2017.06.004
35. Liu G, Zou J, Tang Q, et al. Surface modified Ti(3)C(2) MXene nanosheets for tumor targeting photothermal/photodynamic/chemo synergistic therapy. *ACS Appl Mater Interfaces*. 2017;9(46):40077–40086. doi:10.1021/acsami.7b13421